

Experimental Aerodynamic Control of a Long-Span Suspension Bridge Section using Leading and Trailing Edge Control Surfaces

K. Gouder, X. Zhao, D. J. N. Limebeer, *Fellow, IEEE*, J. M. R. Graham

Abstract

We investigate experimentally the suppression of flutter in long-span suspension bridges. A rigid sectional model of a long-span suspension bridge is mounted in a wind tunnel on a suspension system. Control surfaces, which are used to suppress flutter, are movable flaps that are fitted to the bridge section's leading and trailing edges. The flaps are responsive to the deck's heave and pitch motions. In this work the aerodynamic forcing is modelled using thin aerofoil theory, although other modelling techniques can be used. The controller has a second-order passive transfer function with inputs of a combination of the deck's pitch angle and heave position, and outputs of the flaps' angular positions. The control system design problem is solved as an \mathcal{H}_∞ optimisation problem.

Index Terms

Long-span suspension bridge, wind tunnel experiments, thin aerofoil theory, flutter, buffeting, robust control, control surfaces, flaps.

K. Gouder and J.M.R. Graham are with the Department of Aeronautical Engineering, Imperial College London, London SW7 2AZ, United Kingdom, e-mails: kevin.gouder04@imperial.ac.uk; m.graham@imperial.ac.uk.

X. Zhao is with the School of Engineering, University of Warwick, Coventry, CV4 7AL, United Kingdom, e-mail: xiaowei.zhao@warwick.ac.uk.

D.J.N. Limebeer (Corresponding Author) is with the Department of Engineering Science, University of Oxford, Parks Road, Oxford OX1 3JP, United Kingdom, e-mail: david.limebeer@eng.ox.ac.uk.

Experimental Aerodynamic Control of a Long-Span Suspension Bridge Section using Leading and Trailing Edge Control Surfaces

I. INTRODUCTION

THE structural flexibility of cable-supported bridges [1], and their low structural damping [2], make them susceptible to wind excitation. Potentially unstable modes can be oscillatory or exponentially divergent. The Tacoma Narrows bridge disaster (1940) was caused by the gradual growth, over a period of 45 minutes, of a torsional flutter oscillation [3] due to a sign reversal in the aerodynamic derivative A_2^* related to torsional damping. From the available footage it can be observed that the torsion flutter involved the first asymmetric torsion mode. The continuing need to construct bridges of very long main span faces a major design limiter in the reduction in critical wind speed for the onset of aerodynamic flutter as the span is increased. This constraint has promoted development of methods of raising the critical wind speed for long-span bridges. Usually improvements are made by stiffening the deck structure, particularly in torsion. The depth or the width of the deck may be increased, both of which increase the weight and therefore cost. Adding a spanwise beam, which may be porous, along the deck centre-line, or splitting the deck creating a gap between the two carriage-ways, can add stiffness and, as with modification of the two sides of the deck (the leading and trailing edges), can provide beneficial changes to the aerodynamic derivatives of the deck section, often by influencing the flow separations around the deck, [4]. Fairings added around or beneath the leading and trailing edges can modify the aerodynamic derivatives as well as affecting the vortex shedding from the deck, [5]. Other systems, [6], use a number of main cables and hangers to increase the stiffness of the bridge assembly. All such methods of increasing critical wind speed are based on fixed devices or modifications to the deck cross-section and further significant gains are becoming increasingly difficult

to achieve.

An alternative approach to flutter suppression, which has been under development in the aircraft industry, [7] and [8], is to make use of active devices that respond to the oscillatory motion of the wing. This type of closed loop control, which in aircraft most often uses trailing edge flaps has also been considered as a practical method of raising the critical wind speed for suspension bridges, [e.g. [9], [10], [11]]. COWI A/S have been granted a patent on a system which delays flutter through actively-moving flaps, [12]. Another patent has been granted, [13], for a system of stabilising flaps driven directly by the angular movement between the deck and tensile supports. In the case of bridges, the wind may come from either side. Although in many cases the highest winds will come from one side only, flaps will usually be deployed on both sides, thus both leading and trailing edge flaps should be considered, which may or may not be used simultaneously. Theoretical studies of the application of the technology to cable suspended bridges have been reported in many papers, e.g. [11], [14], [15], [16], and [17]], considering flaps on both sides of the deck.

Theoretical analysis of the unsteady flow field for classical two-degree-of-freedom heave-torsion flutter of bridge deck sections has been shown to give reasonably accurate predictions of the critical flutter speed for thin sections, treated as two-dimensional and elastically mounted, using the unsteady thin aerofoil formulations derived by Theodorsen, [18]. The predictions have been extended to cover thicker and/or bluffer deck sections by modifying the aerodynamic derivatives taking account of measured values over the relevant reduced frequency range where available. Two-dimensional sectional results are normally applied on a strip theory basis for the modal response of the whole span of a three-dimensional bridge on the assumption that all span-

wise variations including geometry, modal displacement and wind speed are gradual, i.e. negligible on a length scale equal to the bridge chord (cross-deck width). This assumption and its implication for aerodynamic load prediction has been discussed in [19], principally for buffet by incident turbulence. This was shown to hold accurately for deck planform aspect ratios, wavelengths of structural modes and length scales of incident turbulence typical for such bridges. The extension of the thin aerofoil analysis (Theodorsen and Garrick, [20]) for the case of a two-dimensional thin aerofoil, flap plus tab system has been applied in [15], using a configuration transformation to predict the aeroelastic response of a bridge deck section fitted with leading and trailing edge flaps. This has demonstrated that closed-loop control of moderate chord flaps has the capability of raising the critical heave-torsion flutter speed of the deck section by a significant amount by changing the aerodynamic stiffness and damping. An added advantage of this type of control is that the control forces, being aerodynamic in origin, scale with wind speed similarly to the excitation forces. [9] reported wind tunnel experiments using aerofoils suspended beneath the deck. The assumption in the analysis of this system is that the aerofoils and bridge deck are aerodynamically independent; this has been shown to be a rather poor assumption in [21] – there is considerable interference unless the aerofoils are an impractical distance away from the deck (> 1 deck width for the trailing edge flap). [22] carried out wind-tunnel testing of a deck section with control flaps governed by a pendulum attached to the bridge deck. For small flap angles, their experiments had good agreement with theoretical predictions but the independent formulation of the aerodynamic forces acting on the deck and flaps, rather than an identification of the coupled aerodynamics of the whole system, led to large discrepancies at large flap angles. [11] reported wind tunnel measurements on a rectangular section deck fitted with triangular leading and trailing edge flaps. This investigation included measurements of aerodynamic damping compared with the predictions of the Theodorsen theory but making a small approximation in the aerodynamics of the leading edge flap. [17] reported a model formulation for control of two piecewise-continuous flaps along the span, each part-flap receiving local feedback. The system is tested through a numerical example but no experimental testing of

the proposed flap control was carried out.

In the present paper we study the flutter suppression of long-span suspension bridge decks experimentally and theoretically using Theodorsen's theory and \mathcal{H}_∞ optimisation. A laboratory scale model of a two-dimensional section of a representative bridge deck was equipped with both leading edge and trailing edge flaps controlled to provide flutter suppression. The nominally rigid model was supported on springs across the wind tunnel working section so as to have response limited to two degrees of freedom (heave and pitch). The scaled frequencies of these two were chosen to be representative of the frequencies of relevant bending and torsion modes of a long-span bridge. The model was wind-tunnel tested mainly under low turbulence conditions. Additional tests were carried out under conditions of grid-generated turbulent flow in order to study the robustness of the controllers under conditions of significant excitation. In such tests, although the turbulence intensity can be reasonably close to the full-scale situation, the ratio of the length scale of the turbulence to the bridge deck chord is always very small in comparison with the same ratio for a full-scale bridge in the atmospheric boundary layer.

The flaps were hinged at the leading and trailing edges of the original unmodified bridge deck and driven by stepper-motors under closed loop control provided by an external computer taking motion data from the bridge deck. The theoretical model of the bridge's sectional aerodynamics was based on Theodorsen's theory for aerofoil + trailing edge flap + tab, transformed to represent a main deck fitted with both leading and trailing edge flaps, simultaneously active. An implementation of each of the controllers used the structural and mass parameters of the wind tunnel model for the dynamics, and therefore results, to compare with the wind tunnel test results. The actual deck section used for the tests was reasonably representative of the more streamlined type of bridge deck section, of an approximately trapezoidal section with small negative camber, and having scaled representative properties as explained in Section IV. The experiments at reduced Reynolds number, which are inevitable in wind tunnel tests, are expected to be conservative, i.e. at this much reduced scale, separations are unlikely to be much less than at full scale. The sectional results may be used to infer the aerody-

dynamic behaviour of a full three-dimensional bridge span on a strip theory basis. For practical reasons, the control flaps for an entire bridge could not be continuous, full-span flaps but would need to be in the form of multiple limited-span flaps deployed in distributed fashion over sufficient lengths around the antinodes of the bending and torsion flutter modes which usually occur in the same region of the bridge deck, and acting under unified control.

The tests were carried out to assess how well the flutter suppression capability was retained in the physical system compared with the theoretical predictions. The flutter derivatives of the experimental bridge deck are used to explain the discrepancies between the theoretical and measured performance of the system, mainly due to the effect of separated flow occurring especially over the trailing edge flap. The flap controllers tested were restricted to low-order passive networks. Passivity implies that the controller can be constructed from passive components such as springs, dampers and inertances.

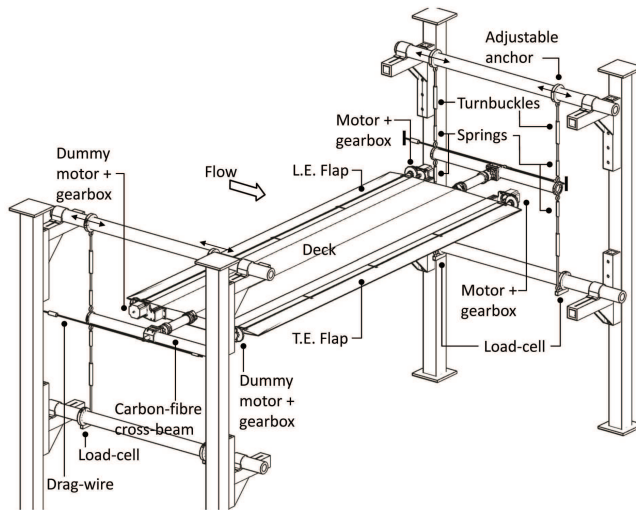


Fig. 1: shows a schematic of the bridge test section. The tunnel walls (or false walls) have been omitted for illustrative clarity.

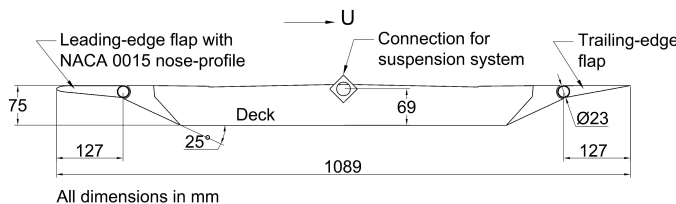


Fig. 2: The 1:50 model deck with dimensions.

The experiments were carried out in two low-speed wind-tunnels using a 1:50 scale thin bridge deck section based on a streamlined box girder design; see Figures 1 to 2. In these experiments, the wind speed was increased in steps up to 15% above the flutter speed of the uncontrolled deck with locked flaps. At each measurement of wind speed the flaps were initially locked, and the flutter oscillations were allowed to build if the deck was unstable. The control system could then be used to suppress flutter for wind speeds of at least 1.25 times the critical (uncontrolled) flutter speed. The controlled flutter speed was obtained by extrapolating the experimental damping ratio characteristic of the deck.

If successful, active flap flutter suppression could potentially be one of the mechanisms facilitating longer spans. The control system could also be deployed as a temporary measure to suppress flutter during bridge construction. The deck is particularly vulnerable during construction, because the deck is not fixed at both ends and the critical flutter velocity is substantially lower (compared with the completed deck) at certain phases of construction [23].

This work is the experimental analogue of earlier theoretical studies [21] and [24], where a simple sectional model with controllable leading- and trailing-edge flaps, having the structural and aerodynamic properties of a long-span suspension bridge was presented. In these references, and in the present paper, the mass and moments of inertia of the flaps are ignored, and the output of the control are the flap angles. The key finding is that the critical wind speeds for flutter of the sectional model can be greatly increased, both theoretically and in a wind tunnel experiment, with good stability robustness. The flaps can be powered by the deck's motion rather than an external power source. In [21] and [24] the Akashi-Kaikyo Bridge was used as the working example for a theoretical study and this work showed that the critical wind speed can be increased to 80 m/s (from 52 m/s) with good robust stability margins.

The structural and aerodynamic components of the model used in this work are presented in Section II. A lumped-mass model of a single bridge deck section with heave and pitch degrees of freedom and two movable flaps is presented in Section II-A followed by an aerodynamic model based on 'thin aerofoil' theory in Section II-B. The control

system design process is discussed in Section III. A description of the experimental setup is given in Section IV. The main results are given in Section V, where the properties of the experimental deck, the experimental and theoretical results are described. A discussion follows in Section VI and a summary of the findings is drawn in Section VII.

II. DYNAMIC MODEL

In the following the structural and aerodynamic models used to study the control of the movable flaps shown in Figure 2 are presented.

A. Structural Model

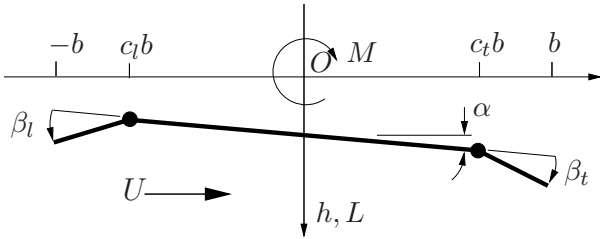


Fig. 3: Kinematic model of the bridge deck with the origin of the inertial axis system at O . Sign conventions: wind velocity U is positive to the right, the heave h and lift force L are positive downwards, the moment M – about the centre-chord – and pitch angle are positive clockwise, the leading and trailing-edge flap angles β_l and β_t are positive when the flaps deflect downwards, i.e. β_l is positive counter-clockwise; β_t is positive clockwise. The deck chord (including flaps) is $2b$. The leading- and trailing-edge flap chords are $(1 + c_l)b$ and $(1 - c_t)b$ respectively; note that c_l is a negative quantity.

The dynamic model of the deck with leading- and trailing-edge flaps is derived using the free body diagram in Figure 3. For this model, the equations of motion for the two degrees of freedom are:

$$M_h(\ddot{h} + 2\zeta_h\omega_h\dot{h} + \omega_h^2h) = L, \quad (1)$$

where M_h is the mass per unit span of deck and L is the lift force. Balancing moments around the deck's mid point gives

$$J_\alpha(\ddot{\alpha} + 2\zeta_\alpha\omega_\alpha\dot{\alpha} + \omega_\alpha^2\alpha) = M, \quad (2)$$

where J_α is the deck moment of inertia about the mid-deck axis per unit span. The structural

damping ratios of the heave and pitch modes are ζ_h and ζ_α respectively, while ω_h and ω_α are their undamped natural frequencies. The aerodynamic lift and moment are a function of the wind speed, as well as of the heave, pitch and flap angles and their derivatives as will be explained in the next section.

B. Aerodynamic Model

The aerodynamic model is based on the wing-flap-tab combination considered under the assumptions of thin aerofoil (small perturbation) theory in Theodorsen and Garrick, [20]. The lift on the system is given by

$$L = \rho b^3 \omega^2 \left\{ L_h \frac{h}{b} + L_\alpha \alpha + L_{\beta_t} \beta_t + L_{\beta_l} \beta_l \right\}, \quad (3)$$

while the moment is given by

$$M = \rho b^4 \omega^2 \left\{ M_h \frac{h}{b} + M_\alpha \alpha + M_{\beta_t} \beta_t + M_{\beta_l} \beta_l \right\}. \quad (4)$$

The quantities L_h , L_α , L_{β_t} and L_{β_l} are lift-related aerodynamic derivatives, while M_h , M_α , M_{β_t} and M_{β_l} are moment-related aerodynamic derivatives corresponding to the various perturbation variables. These derivatives are functions of the Theodorsen function $C(k)$ given by

$$C(k) = \frac{J_1(k) - jY_1(k)}{(J_1(k) + Y_0(k)) - j(J_0(k) - Y_1(k))}, \quad (5)$$

in which $J_0(k)$, $J_1(k)$, $Y_0(k)$ and $Y_1(k)$ are Bessel functions of the first and second kind respectively, $k = \omega b/U$ is the reduced frequency [25] and $j = \sqrt{-1}$. The Theodorsen function is an irrational function of the reduced frequency and it is convenient, for computational reasons, to approximate it and other irrational quantities with low-order rational functions. An accurate quartic approximation of $C(k)$ first derived in [21] is given in Table I.

numerator terms	denominator terms
0.99592	1
57.01896 \hat{s}	62.30441 \hat{s}
623.78848 \hat{s}^2	807.78489 \hat{s}^2
1895.46328 \hat{s}^3	3060.67868 \hat{s}^3
1523.24700 \hat{s}^4	3033.76379 \hat{s}^4

TABLE I: Theodorsen function: numerator and denominator coefficients of a quartic approximation.

Here $\hat{s} = \frac{sb}{U}$ is the reduced Laplace transform variable; the reduced frequency is given by $k = \text{Im}(\hat{s})$. Since linear thin aerofoil theory is assumed, superposition can be used to transform the wing-flap-tab combination into a bridge deck fitted with leading- and trailing-edge flaps. This transformation is illustrated in Figure 5 with further detail given in [21]. The heave and pitch corrections mentioned in the caption of Figure 4 involve replacing h by $h + c_l b \beta_l$, and replacing α by $\alpha - \beta_l$, the first and second derivatives of h and α are adjusted similarly in (22)-(25) of [20]. This procedure has been checked in [21] against a vortex panel numerical method, which makes the thin aerofoil assumptions, and excellent agreement is demonstrated.

III. CONTROL SYSTEM DESIGN

Figure 5 shows the bridge feedback control system. The uncontrolled open-loop system (i.e. the deck and flaps) is described by the plant $P(s)$ that contains the structural dynamics and the non-circulatory part of the fluid mechanics, and the Theodorsen function approximation $C(s)$ that generates the circulatory flow. The control system $K(s)$ consists of three parts:

$$K(s) = G_f(s)G_c(s)G_m(s) \quad (6)$$

where $G_c(s)$ is the controller, $G_f(s)$ is the low-pass filter which is used to filter out noise in the feedback signals at frequencies well above those of the bridge dynamics, and $G_m(s)$ is the stepper motor. $K(s)$ can be SISO to drive one flap or MIMO to drive both flaps, which has input of bridge position(s) and output of flap angle(s). Correspondingly $G_c(s)$ denotes either the trailing-edge controller, leading-edge controller or both, and both have the form

$$\frac{ks}{s^2 + 2\zeta\omega_n s + \omega_n^2} \quad (7)$$

where $k, \zeta, \omega_n > 0$. As shown in [26], the corresponding Bode plot is bell shaped which can eliminate noise and allow flaps to operate around their zero positions. Similarly, $G_m(s)$ denotes either the trailing-edge motor $G_t(s)$ or leading-edge motor $G_l(s)$ or both, which are

$$G_t(s) = \frac{s + 78.3819}{s + 76.0316} \quad \text{and} \quad G_l(s) = \frac{s + 0.4771}{s + 0.2990}$$

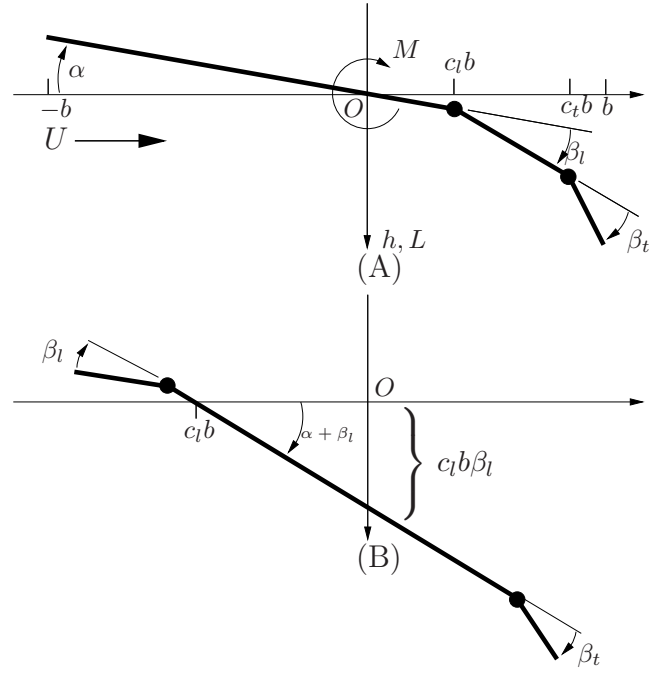


Fig. 4: Transformation of the Theodorsen-Garrick wing-aileron-tab configuration [20] into a controlled bridge deck. In (A) the wing pitch angle is α , the aileron angle is β_l and the tab angle is β_t . The wind speed is U (from the left), the heave h and lift L are positive downwards, while moments and angles are positive clockwise. The wing chord is $2b$, and the width of the tab and aileron are described in terms of c_t and c_l respectively. In (B): The wing-aileron-tab configuration is transformed into the double-flapped bridge deck by making c_l negative, thereby forcing the flap hinge to the left of the origin [21]. In this new configuration the aileron becomes the bridge deck, the wing the leading-edge flap and the tab the trailing-edge flap. In order to re-level the bridge, and return its mass centre to correct position, pitch and heave corrections must be applied.

respectively. These transfer functions were determined in wind tunnel experiments using a motor-gearbox-flap system identification process with chirp, or white noise excitation sequences.

The generalised state-space model of the uncontrolled open-loop system is of the form

$$E\dot{x} = Ax + Bu \quad (8)$$

$$z = Cx, \quad (9)$$

which is an assembly of equations (1), (2), (3), (4) and (5). The state-space model of $P(s)$ can be easily obtained from the ordinary differential model

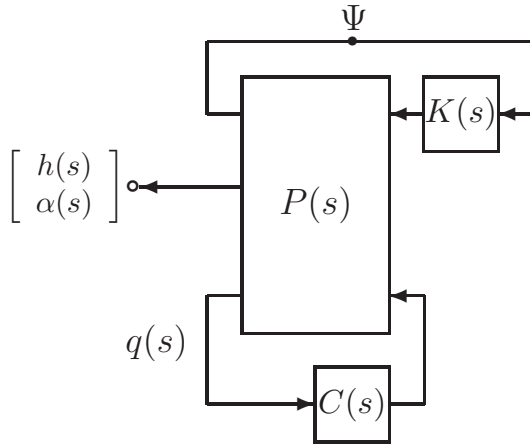


Fig. 5: Block diagram of the aeroelastic control system. The dynamics of the bridge and non-circulatory fluid mechanics are represented by the plant $P(s)$, a rational approximation to the Theodorsen circulation function approximation is given by $C(s)$. $q(s)$ is the vertical velocity of the air stream relative to the structure. The flap control system is given by $K(s)$ and the feedback signal by Ψ .

(1), (2), (3), (4) excluding the terms containing Theodorsen function, with input of force/moment generated by the circulatory flow and output of q (vertical velocity of the air stream relative to the structure). The state-space model of $C(s)$ can be obtained from its transfer function in Table I. Then (8) - (9) can be derived easily by the interconnection of the state-space models of $P(s)$ and $C(s)$. The input(s) and output(s) of (8) - (9) are the flap angle(s) and bridge position(s) respectively.

The root locus of the plain deck is shown in Figure 6, where it is observed that the critical flutter speed of the theoretical model is 20 m/s, while its critical torsional divergence speed is 24 m/s. The design aim is to increase the theoretical critical flutter speed to 24 m/s.

A simple multiplicative representation of stability robustness is used for optimisation purposes [27]. To this end we seek a passive network that stabilises the nominal closed loop and achieves the following closed-loop robust min-max objective:

$$\min_p \left\{ \max_{Q_i(s,p)} \left\| (I + Q_i(s,p))^{-1} \right\|_{\infty} \right\} \quad i = 1, \dots, n, \quad (10)$$

where the multi-variable transfer functions $Q_i(s,p) = K(s)C_i(sE - A_i)^{-1}B_i$ are open-loop transfer functions corresponding to wind speeds

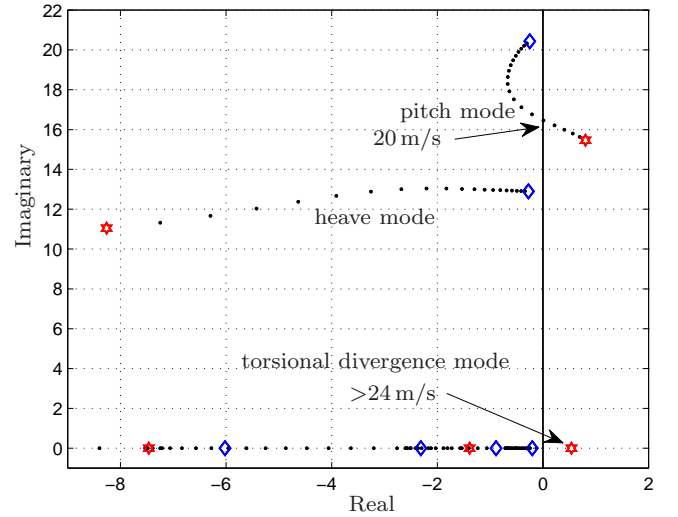


Fig. 6: Root-loci of the uncontrolled bridge section. The wind speed is swept from 5 m/s to 25 m/s, with the low-speed end of the root loci marked with (blue) diamonds and the high-speed ends marked with (red) hexagons. The (flutter) pitch mode goes unstable at approximately 20 m/s, while the torsional divergence mode goes unstable at approximately 24 m/s.

U_i $i = 1, \dots, n$ (from 4 m/s to 24 m/s in steps of 5 m/s), which are obtained by opening the feedback loop at Ψ in Figure 5. E , A_i , B_i , C_i are as in equations (8) and (9) corresponding to U_i . The Laplace transform variable is denoted s and $\|\cdot\|_{\infty}$ is the frequency-response infinity norm [27]. The aim of this performance criterion is to maximise the closed-loop robust stability margin relative to the multiplicative model error for all the wind speeds considered because ultimately we need to control a physical bridge deck instead of its theoretical model. The compensator parameters in (7) are stored in p , which are optimised using the MATLAB sequential quadratic programming algorithm FMINCON [28] with a constraint that the real parts of the closed-loop eigenvalues are negative (i.e., the closed-loop system is ensured to be stable).

A sample of the optimal compensators found by FMINCON are summarised in Table II. With these control systems, the robust performance criterion (10) has values of 1.3364, 1.9621, 2.7729 and 2.0696 respectively. Their root locus diagrams are shown in Figures 7 - 10, which indicate that the heave, pitch and torsional divergence modes are all

well damped up to $U = 24$ m/s. This means that all the controllers achieve at least 20% improvement to the critical wind speeds in the theoretical model. We expect that all these robust controllers should also achieve similar improvements in critical wind speeds in wind tunnel tests as these controllers are designed to handle modelling error and uncertainty.

#	Flap(s)	Controller
1	LE : α	$\frac{-32.8185s}{s^2 + 5.5575s + 182.667}$
2	LE, TE : α	TE: $\frac{-30.6882s}{s^2 + 18.6616s + 310.4151}$ LE: $\frac{-70.9502s}{s^2 + 130.2945s + 149.7662}$
3	LE : α , TE : h	TE: $\frac{-79.126s}{s^2 + 32.6885s + 157.1237}$ LE: $\frac{-58.3121s}{s^2 + 11.6757s + 81.5644}$
4	TE : α	$\frac{-30.6758s}{s^2 + 16.278s + 328.7332}$

TABLE II: Controllers tested with their operating flaps and feedback signals. The abbreviations LE and TE denote the leading- and trailing-edge flaps, while α and h denote pitch and heave feedbacks. The gain for each controller is equal to 1; when a higher gain is mentioned, this implies a linear multiplier (= gain value) of the output flap angle.

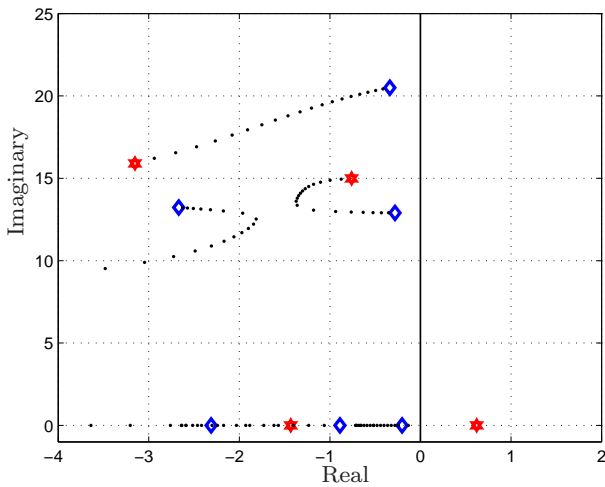


Fig. 7: Root locus for the bridge section with Controller #1 in Table II. The wind speeds and symbols follow Figure 6.

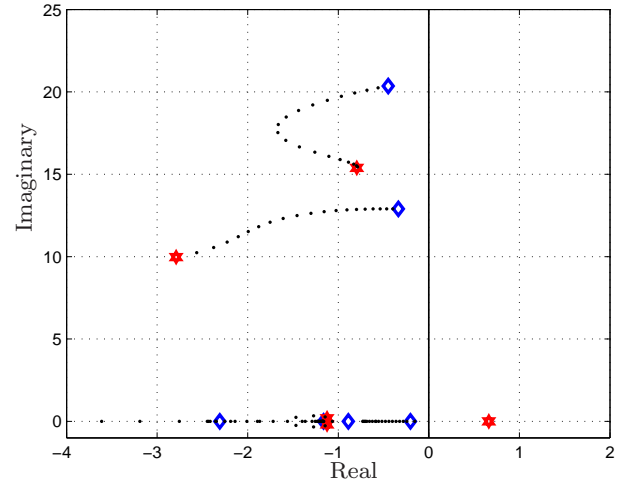


Fig. 8: Root locus for the bridge section with Controller #2 in Table II. The wind speeds and symbols follow Figure 6.

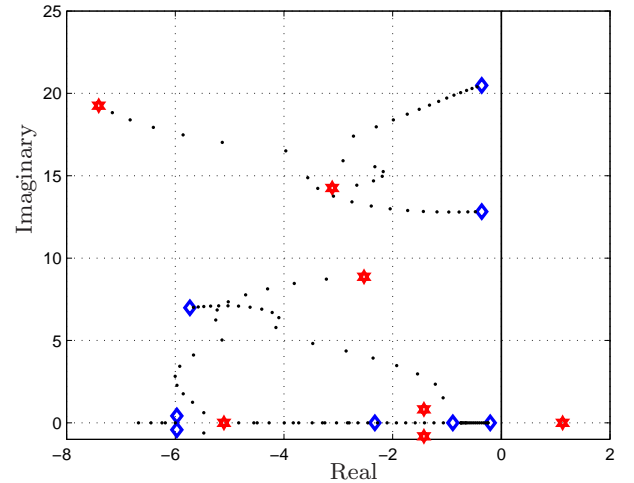


Fig. 9: Root locus for the bridge section with Controller #3 in Table II. The wind speeds and symbols follow Figure 6.

IV. EXPERIMENTAL SETUP

The main deck utilised in these experiments is a rigid carbon-fibre-composite structure of chord 0.82 m, span 2.74 m and depth 0.075 m. This model has the cross-section of a prototypical bridge deck that had previously been used for wind tunnel testing at BMT Fluid Mechanics Ltd. The deck's trailing and leading edges were both faired using low-density styrofoam prior to the installation of flap-type control surfaces. The total deck chord, including the fairings and the flaps, was 1.09 m and each of the flaps had a chord of 12% of the

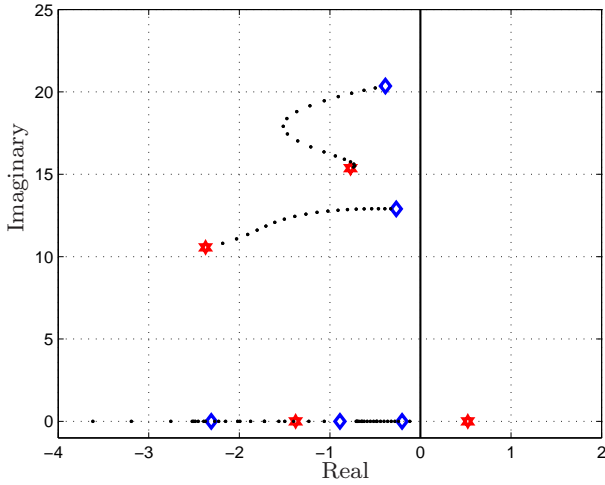


Fig. 10: Root locus for the bridge section with Controller#4 in Table II. The wind speeds and symbols follow Figure 6.

total deck chord. Both flaps were initially of a thin triangular section, but the leading edge flap was eventually made less sensitive to angle of attack by giving it a NACA0015 nose profile to suppress the leading edge separation that would otherwise occur. Each of the flaps was mounted onto an aluminium-alloy tube and connected to a 1:5 reduction spur gear gearbox driven by a Nanotec ST8918S4508 NEMA34 stepper motor capable of developing up to 3 Nm of torque. The motor was controlled using the Nanotec SMC147-S Stepper Motor Positioning Controller. System setup was performed through a serial communication link with a control computer. The motor was run in the Analogue Positioning mode; the motor position was proportional to an analogue voltage input to the SMC147-S. The SMC147-S ran an internal PID controller in hardware that governed corrections to ensure shaft positional fidelity to the analogue input voltage demand. The PID controller's parameters were set prior to the experiment by running an internal PID parameter wizard on the SMC147-S. Shaft positional feedback was attained through a WEDS5541-B shaft encoder, which has 4000 counts per revolution in quadrature. The continuous flutter controllers were converted to discrete time versions and implemented in a Labview control program.

The deck spanned the BMT tunnel No. 5, which has a working section of width 2.74 m and height 2.7 m. The motors and gearboxes are fitted to one end of the deck section, with balancing counter

weights fitted at the other end. Both were outside the tunnel walls; see Figure 1. Experiments were also conducted in the Honda wind-tunnel at Imperial College, which has a working section of width 3 m and height 1.5 m. In this case false walls were utilised because this tunnel test-section is wider than the length of the model deck section. The motors and gearboxes were situated between false walls and the Honda tunnel walls. A suspension system was designed and assembled either side of the tunnel test section, at both the BMT and the Honda tunnels. This consisted of an H-assembly of springs that allowed the deck torsional and heave degrees of freedom. Spanwise and streamwise sway was constrained with drag wires. The deck's roll freedom was unconstrained, but with the deck spanning the wind-tunnel, the aerodynamic forces were largely two-dimensional and hence the excitation of this mode was negligible. The full-scale representative prototype had bending frequency ≈ 0.29 Hz and torsional frequency ≈ 0.45 Hz. The Froude number was not matched since this only becomes important when part of the structural stiffness is provided by gravitational forces, as is the case when full model testing of suspension bridges is carried out, [29]. Therefore the frequency ratio of the model was made equal to the full-scale prototype's = 1.54. The mass ratio $\frac{M_h}{\rho A_x} \approx 190$ (where M_h is the deck mass per unit length and A_x is an area defined as deck chord $2b \times$ deck depth) was also matched to the full-scale representative prototype. The Reynolds number based on the deck width (chord) was just above 1×10^6 . The heave frequency was set by using a set of eight springs forming the two H-assemblies; each of the springs had a stiffness of 1160 N/m. With the heave frequency set, the frequency ratio could be set by adjusting the horizontal distance between the springs, hence adjusting the torsional frequency. The deck was balanced, i.e. it had no static moment and hence the term a in equations XVIII-XX in [18] is zero. The deck experienced a small mean aerodynamic moment, since the aerodynamic centre was close to the quarter chord of the deck. This, coupled with a negative camber and some separated flow, induced a small mean incidence. The drag wires were connected at the point of torsional rotation through low-stiffness leaf springs in order to minimise the introduction of any additional damping. The structural damping ratios were $\zeta_h = 0.0057$ and $\zeta_\alpha = 0.0033$, or in log-

dec format, $\delta_h = 0.036$ and $\delta_\alpha = 0.021$.

Each of the springs at the bottom of the H-assembly legs were connected to a MIL-LB-8000 load cell driven by a full-bridge amplifier from Fylde. Measuring the reaction loads, and knowing the stiffness of the suspension system springs, enabled the direct acquisition of the bridge deck's heave and pitch positions. The bridge deck's positions were acquired on the analogue input channels of an NI PCI-6259 data acquisition card, while the motor's shaft position was acquired on digital counter channels. The motor's position demand appeared on the analogue output channels.

The parameter values for the experimental deck are given in Table III. These parameters will be used in the structural model (II-A) and aerodynamic model (II-B).

Parameters	Values
b	0.545 m
M_h	18.9 kg
J_α	1.8 kg m^2
ω_α	20.74 rad/s
ω_h	13.45 rad/s
ρ	1.23 kg/m^3

TABLE III: Physical parameters of the deck used in the current experiment. The semi-chord b stated here includes the flap chords.

For the purpose of theoretical predictions the flaps and bridge deck are treated as aerodynamically 'thin'. The flap resonant frequencies about their hinge lines, ω_{β_l} and ω_{β_t} , respectively, were chosen so that the flaps are stable for wind velocities well beyond the velocities tested here, and hence will not decrease the critical wind speeds for flutter and torsional divergence in the absence of flap controllers.

A first approximation of the flutter velocity was obtained using Selberg's flutter velocity prediction formula, [30],

$$U_{flut} = 3.71 \cdot f_\alpha \cdot 2b \cdot \sqrt{\frac{\sqrt{M_h J_\alpha}}{\rho (2b)^3} \left(1 - \left(\frac{f_h}{f_\alpha}\right)^2\right)} \quad (11)$$

and the parameters in Table III giving $U_{flut} \approx 19.4 \text{ m/s}$.

This flutter velocity agreed well with those predicted by a Theodorsen thin-aerofoil theory code and a vortex-panel code; both predicted a flutter velocity of 20.1 m/s. Reference is made here to

Table 8.1 in [1], where typical ratios, λ , between the critical flutter wind velocity of typical bridge deck sections and the corresponding critical flutter wind velocity for a flat plate having the same mass, natural frequencies and damping ratios is given.

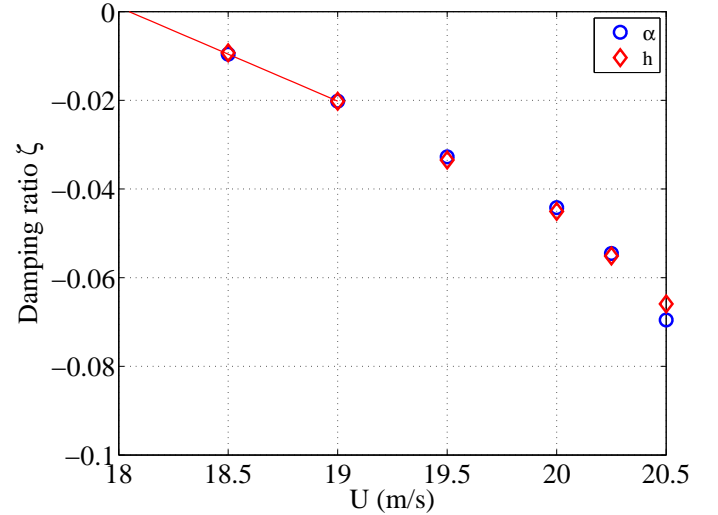


Fig. 11: Damping ratio ζ (for pitch and heave) as a function of the freestream velocity for (supercritical) velocities beyond flutter. The growth trace in each experiment was analysed and the damping ratio evaluated. Extrapolating the linear fit to $\zeta = 0$ gave the critical flutter velocity as approximately 18.05 m/s. This is in contrast to the value of 17.5 m/s obtained if subcritical data below the flutter condition is extrapolated.

For a streamlined box-girder section, similar to that of the deck model used in these experiments, the ratio λ is in the range 0.8 – 0.9 placing the expected experimental flutter velocity in the range 16 – 18 m/s. Figure 11 shows the system damping as a function of wind speed, and predicts zero damping at the flutter velocity of approximately 18.05 m/s. All the data in Figure 11 are from supercritical experiments $U > U_{flut}$ (indicative of negative damping). Each experiment involved initially keeping the deck stable using controlled flaps, and then opening the flap control loop and allowing growth to occur naturally. An exponential-sinusoidal function least-squares fit with four variables (amplitude, phase, frequency and damping ratio) was then applied to the growth traces to identify the damping ratio in each case. Pitch position data was used and the growth trace portion selected for fitting was limited to approximately $|\beta| < 0.006 \text{ rad}$ (≈ 0.5

degrees). It is interesting to note that when the model was perturbed in sub-critical wind velocities, $U < U_{flut}$ and decaying traces were measured, a flutter velocity of approximately 17.5 m/s was identified from the zero intercept of a line through the damping ratio data. In these cases, the bridge deck was given combined heave (≈ 0.01 m) and pitch ($\approx 0.7^\circ$) displacement using a cable pulled by an electromagnet and then released at various sub-critical velocities. At a velocity of 17.5 m/s, the deck oscillations never grew naturally from a stationary start-point, but if the deck was given a displacement and released at the same velocity, then divergent oscillations resulted. This suggests that at velocities close to the critical flutter speed, a finite amplitude displacement is needed to initiate a dynamic instability. The difference between the measured flutter velocity in the Honda tunnel and the BMT tunnel No. 5 was within 0.1 m/s.

The first design aim is to increase the critical flutter speed to a value just below the static divergence speed, which can be computed using:

$$U_{div} = \sqrt{\frac{4K_\alpha}{\rho(2b)^2 \frac{dC_M}{d\alpha}}} \quad (12)$$

where K_α is the torsional stiffness per unit length, $2b$ is the deck chord, $dC_M/d\alpha$ is the slope of the static aerodynamic moment coefficient. From $\omega_\alpha = \sqrt{\frac{K_\alpha}{J_\alpha}}$ and data from table III, $K_\alpha = 774.3$ Nm/rad.

The static tests in Figure 12 show the values of $dC_L/d\alpha$ and $dC_M/d\alpha$ to be 4.95 and 2.61, respectively. As expected, these values were somewhat lower than the theoretical values predicted by thin aerofoil theory of 2π and π respectively. These reductions are due mainly to the effects of operating with a separated flow over the trailing edge. This rear separation also decreases significantly the aerodynamic effectiveness of the trailing edge flap below the value given by thin aerofoil theory. The normalisation performed on the measured lift and moment per unit span, in accordance with the convention used in [18], retains the standard aeronautic normalisation for the lift coefficient but defines the moment coefficient with half the standard normalisation:

$$\text{Lift}(\alpha) = \frac{1}{2} \left(\frac{dC_L}{d\alpha} \alpha \right) \rho \cdot 2b \cdot U^2 \quad (13)$$

$$\text{Moment}(\alpha) = \frac{1}{2} \left(\frac{dC_M}{d\alpha} \alpha \right) \rho \cdot 2b \cdot b U^2. \quad (14)$$

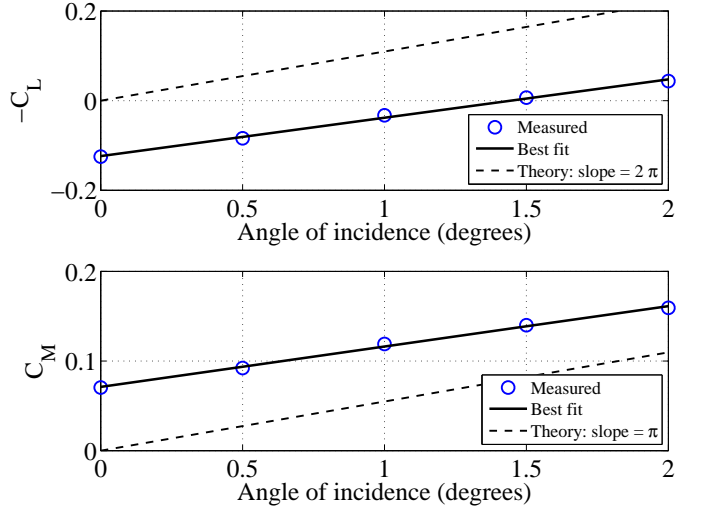


Fig. 12: Lift and Moment acting on the bridge deck in response to a change in deck angle of incidence (angle of attack). The static derivatives $dC_L/d\alpha$ and $dC_M/d\alpha$ were identified from these plots. The data were obtained at a sub-critical velocity of 17 ms^{-1} . The offset between experimental and theoretical trends is due to the deck camber.

Using the theoretical and experimental values for $dC_M/d\alpha$ of π and 2.61, respectively, to calculate the torsional divergence velocity from (12) gives values of 26 m/s and 28.5 m/s respectively.

V. RESULTS

The controllers listed in Table II were tested in the wind tunnel for a range of wind speeds. With one exception the incident wind was uniform and nominally free from turbulence. As shown in Table II, the controllers are all second order, and applied to the leading or trailing edge flap alone, or to both flaps simultaneously. The measured feedback comes from either the deck pitch (α), or from the deck heave (h), or from a combination of the two. In the majority of cases the gain of the leading-edge flap actuator was set to 1, while for the trailing-edge controllers the actuator gain is set to one of 2, 3 or 4 to compensate for the fact that it is operating in the separated near-wake of the bridge deck, observed in flow visualisation and in deck pressure measurements. The reduced performance of the trailing edge flap observed in the static measurements was confirmed when the lift and moment derivatives $\frac{dC_L}{d\beta_t}$ and $\frac{dC_M}{d\beta_t}$ were measured in unsteady flow. This is discussed in detail in Section VI.

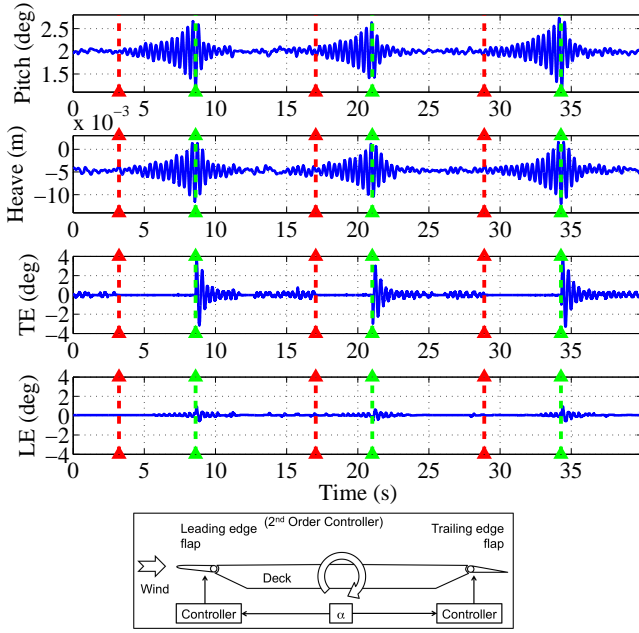


Fig. 13: Controller#2: Time-traces of pitch and heave positions of the deck, and trailing- and leading-edge flaps angles. The gain of the trailing edge flap actuator is 3. The freestream velocity is 20 m/s. The control loop is initially open and the deck motion is allowed to grow naturally. The feedback loop is then closed to suppress any motion.

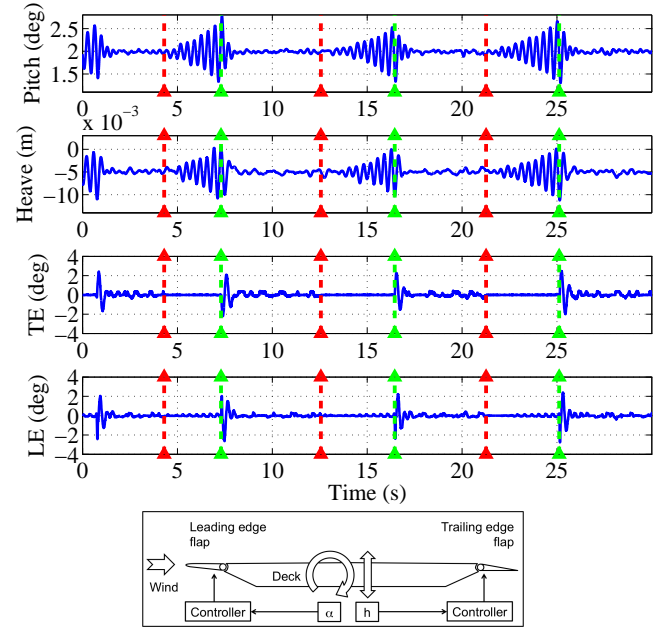


Fig. 14: Controller#3: Time-traces of pitch and heave positions of the deck, and the trailing- and leading-edge flaps angles. The leading-edge flap has deck pitch feedback, while the trailing edge flap has deck heave feedback. The gain of the trailing edge flap actuator is 3. The operating conditions are the same as those in Figure 13.

Figures 13 and 14 show examples of the results of applying the controllers listed in Table II for a super-critical freestream flow velocity of 20 m/s. The critical flutter speed was identified earlier as being in the range 17.5 - 18.05 m/s (depending on whether sub-critical or super-critical data was used in its identification). In each of these figures, time histories of the bridge deck's pitch, heave, and trailing- and leading-edge flap angles are given. When the control is toggled open, indicated by a vertical red dashed line, the flaps are held rigid relative to the deck and the deck experiences growth in its heave and pitch motions. When the control system is subsequently toggled closed (marked with a vertical green dashed line), the flaps apply corrective controls, and the deck heave and pitch displacements are damped.

Figure 14 corresponds to Controller#3 in Table II and shows the performance of a controller in which the leading-edge controller received pitch position feedback, while the trailing-edge controller received heave position feedback. This combination exhibits strong damping properties for flutter and proved to

be one of the best controller arrangements tested. This is demonstrated in more detail in Section VI.

The same controller#3 was further tested in a turbulent flow field in order to study the robustness of the controller under conditions of significant excitation. A bi-planar grid was mounted at the beginning of the test-section approximately 3 m upstream of the bridge deck. At the deck's mid-chord streamwise location, the vertical velocity turbulence intensity $\frac{\sqrt{w^2}}{U}$ was 6.5% and the ratio of spanwise length-scale to deck chord $L_w(y)/2b$ was approximately 0.05, which is very small compared with typical values (>2) for a full scale bridge deck in atmospheric boundary layer turbulence. Figure 15 shows that the controller is still able to suppress flutter in the presence of additional buffet forces. The leading-edge flap exhibits a noisier neutral, 'parked' position when the control loop is toggled open due to it being acted upon by large buffeting forces that prompt continuous corrections by the flap drive-motor. The growth of both the pitch and heave displacements due to the flutter instability is also

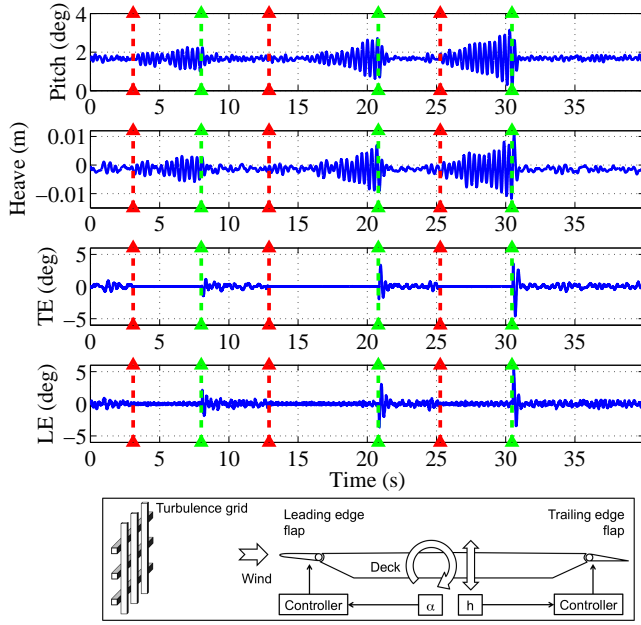


Fig. 15: Controller#3 in turbulent flow: the controller based on a trailing-edge flap receiving heave feedback and a leading-edge flap receiving pitch position feedback. The gain of the trailing edge flap actuator is 3 and the freestream velocity is 19 m/s.

noisier due to superimposed buffet-induced motions. Controllers specifically designed to alleviate buffet-induced forces have also been tested for flutter suppression and are discussed in detail elsewhere [31].

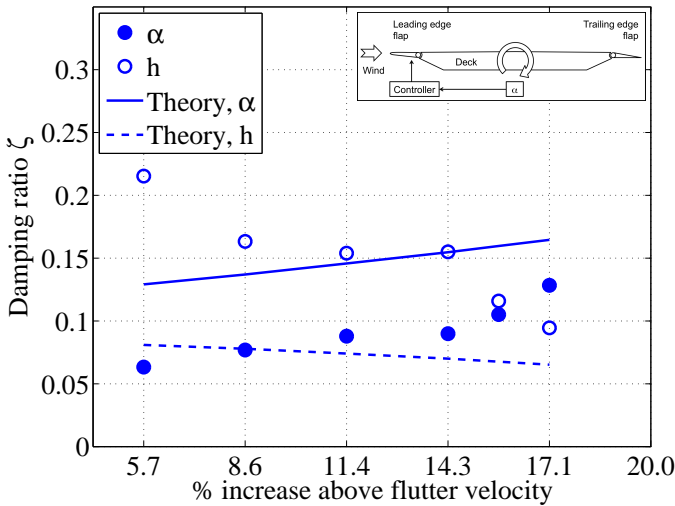


Fig. 16: The evolution of the closed-loop ζ as a function of %velocity increase above the flutter velocity for Controller#1.

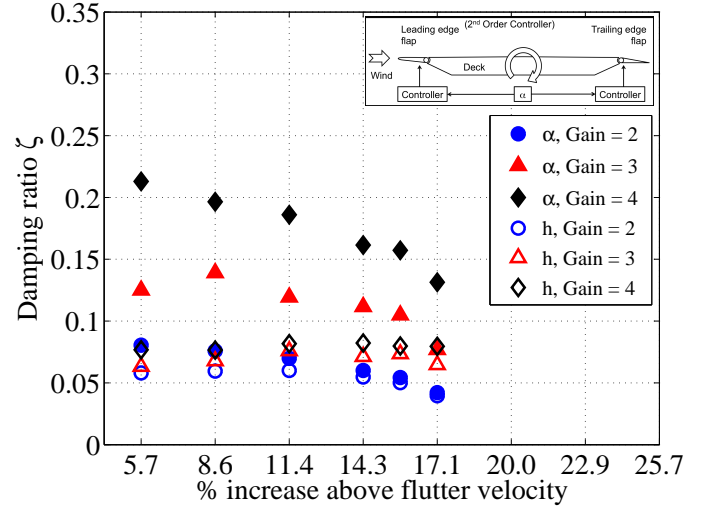


Fig. 17: The evolution of the closed-loop ζ as a function of %velocity increase above the flutter velocity for Controller#2. The gain of the trailing-edge flap is varied from 2 to 3 to 4 at each velocity.

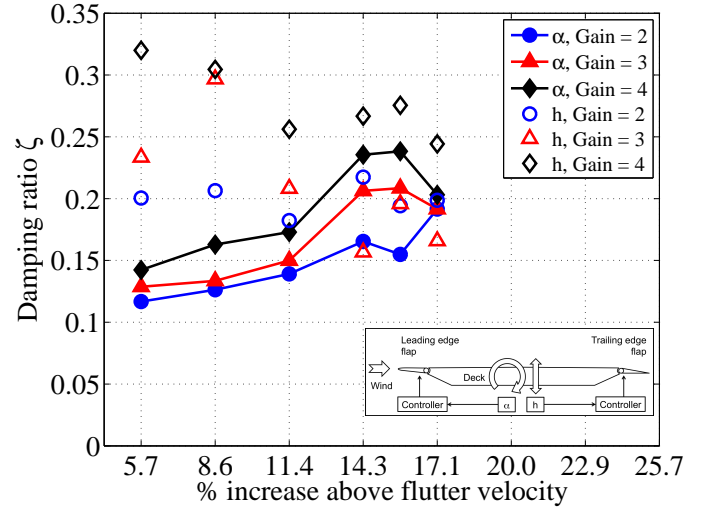


Fig. 18: The evolution of the closed-loop ζ as a function of %velocity increase above the flutter velocity for Controller#3. The gain of the trailing edge flap actuator is varied from 2 to 3 to 4 at each velocity. This controller, which receives both the pitch and heave position feedbacks is the most effective at delaying flutter. The data are connected for illustrative clarity.

Each of the four controllers in Table II were tested for a range of super-critical wind-speeds. At each wind-speed the performance of the controller was assessed through a control-OFF-ON sequence as explained in Figures 13 and 14. The step-response

of each of the controllers was also investigated by allowing the controller to remain ON, while applying a finite combined pitch and heave initial displacement and then releasing the deck. In either case, the decay in oscillations was studied. The controller's effectiveness was quantified by identifying the damping ratio associated with the deck's (second order) response under closed-loop conditions. The time-histories of the damped pitch and heave displacements of the controlled deck are fitted to a curve of the form:

$$X(t) = A_0 e^{-\zeta \omega_n t} \cos(\omega_d t - \phi) \quad (15)$$

in which $X(t)$ represents either the pitch or heave displacement, A_0 is an initial amplitude, ω_n and ω_d are respectively, the undamped and damped natural frequencies of the oscillation, ζ is the damping ratio and ϕ a phase angle. A least-squares fitting script was implemented in MATLAB, which extracted the values of A_0 , ζ , ω_n and ϕ for the best fit. An indication of the goodness of fit is given by the norm of the error, $L_\infty(\alpha_{measured} - \alpha_{fit})$ which was within 0.09 degrees in all cases. The value of ζ was then plotted against %increase in freestream velocity above flutter as shown in Figures 16 to 19.

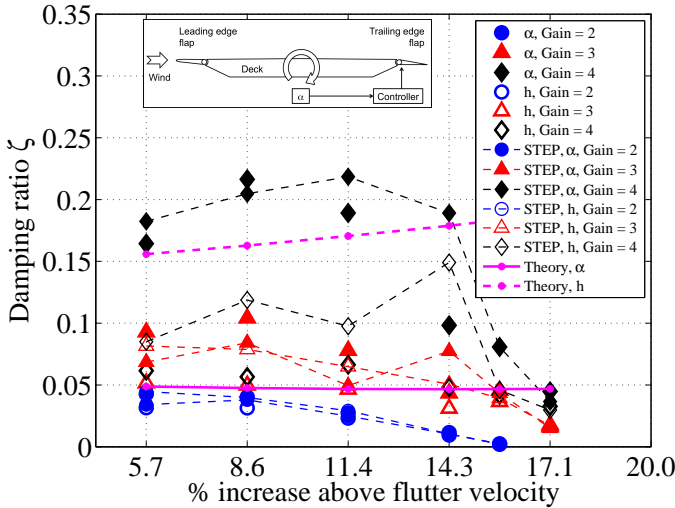


Fig. 19: The evolution of the closed-loop ζ as a function of %velocity increase above the flutter velocity for Controller #4, for gain = 2, 3, 4 at each velocity. For a gain of 2, the increase in critical flutter speed, established by extrapolation, is close to 15%; it is higher for higher gain. The data joined by dashed lines were obtained from a step-response experiment (as opposed to an OFF-ON experiment).

The substantial damping introduced by the evaluated controllers, may be compared with a damping ratio of 0.005, which is typical of structural damping. When compared to the theoretical values of the damping ratio extracted from the root locus Figures 7 to 10, the experimental values do not match exactly. However the trends are similar and the experimental controllers increase the flutter velocity by a similar percentage to their theoretical counterparts, despite the 'thin deck' assumption. For example Figure 16 shows pitch damping increasing and heave damping decreasing with increasing freestream velocity, similarly indicated by theory. Figure 19, apart from highest gain and velocity combinations, shows a slowly decreasing pitch damping and slowly increasing heave damping for all gains, similar to theoretical trends but with experimental gains larger than theoretical.

In Figure 20, we plot the evolution of the damping ratio with %increase above the flutter velocity for all the controllers considered for a trailing-edge actuator gain of 4. The control system using pitch angle feedback of the leading-edge flap and heave feedback on the trailing-edge flap is most effective in delaying the onset of the flutter instability.

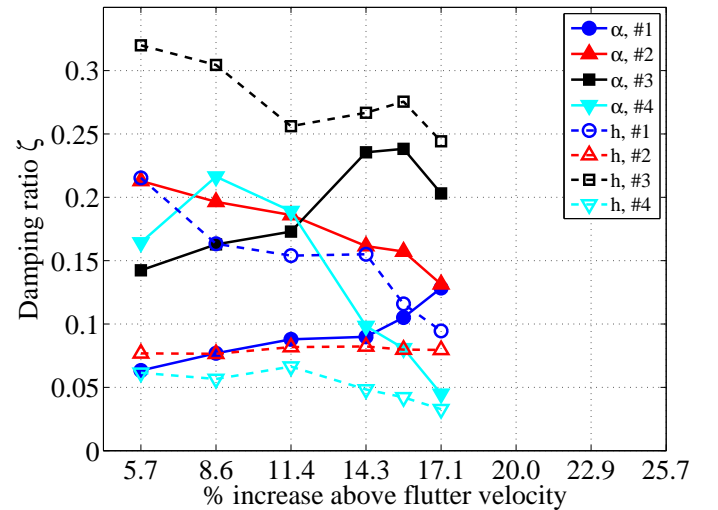


Fig. 20: Evolution of the measured ζ as a function of the %increase above the uncontrolled deck's flutter velocity for each controller considered. The gain for the trailing edge flap actuator is 4 in all cases. The pitch-mode data are joined with solid lines, while the heave-mode data are joined with dashed lines.

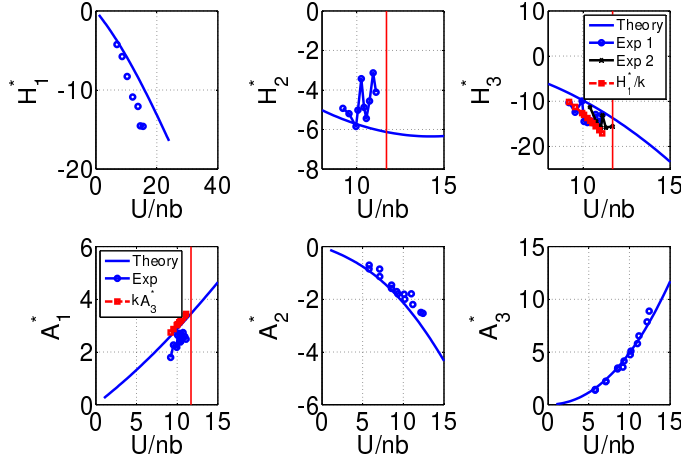


Fig. 21: Aerodynamic derivatives extracted from thin aerofoil theory (solid line), with their experimental counterparts for the experimental deck. The vertical red line corresponds to the flutter velocity and $U/nb = 2\pi/k$ [32]. H_3^* and A_1^* have also been derived from H_1^* and A_3^* respectively, [33].

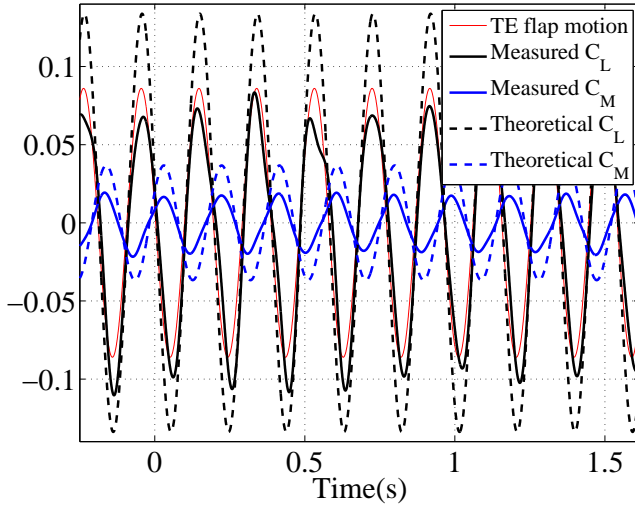


Fig. 22: Measured and predicted lift and moment coefficients in response to trailing-edge flap oscillating at 2.6 Hz and amplitude $\pm 5^\circ$ at a wind-speed of $U = 16$ m/s. The reduced measured C_L and C_M values indicate the flap's reduced effectiveness.

VI. DISCUSSION

Thin aerofoil theory [18] has been used to design flutter suppression controllers. In order to justify this, the derivatives of the deck model were extracted using the method described in [32], and are compared with the theoretical predictions in

Figure 21. Following their procedure, the directly observed derivatives (H_1^* , A_2^* and A_3^*) (through restrained single mode, heave or pitch oscillations) and the indirectly derived derivatives (A_1^* , H_2^* and H_3^*) (through coupled heave and pitch oscillations) were obtained. Fair agreement was observed between the theoretical and measured derivatives. The indirectly derived derivatives A_1^* and H_3^* were also derived using the mutual dependence relationships reported in [33], i.e. $H_1^* = kH_3^*$, $A_1^* = kA_3^*$ and plotted in Figure 21 too. In sum, the fair similarity between the experimentally derived derivatives and their theoretical counterparts from thin aerofoil theory justifies the use of the theoretical model in controller design. This would especially hold true for bridge decks which are streamlined or quasi-streamlined, but would be less suitable to use for very bluff deck sections. In the current case, no correction has been made to account for any disagreements between the predicted and measured main deck derivatives. The influence of the deck's

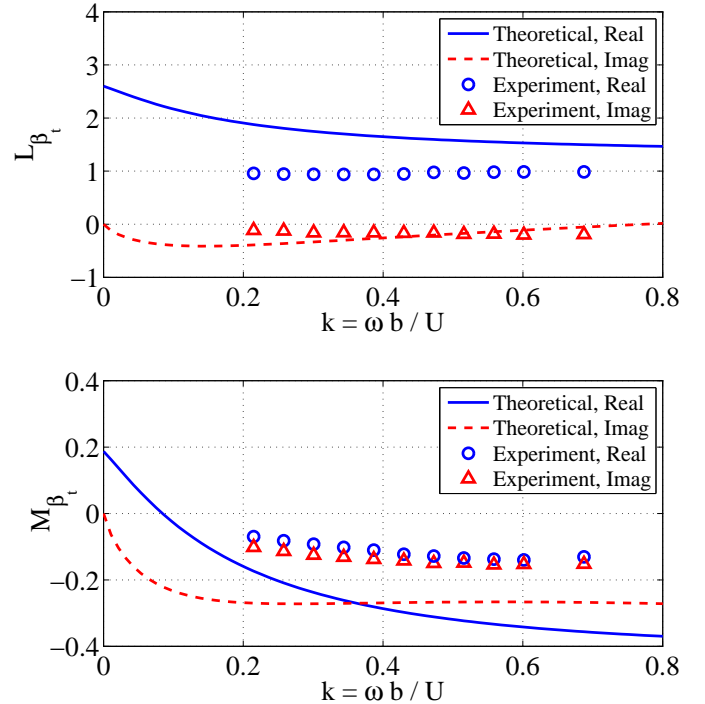


Fig. 23: The real and imaginary parts of the trailing edge flap derivative for various reduced frequencies indicating its reduced effectiveness.

wake on the efficacy of the trailing-edge flap was investigated experimentally. The deck was mounted on load-cells in order to measure the lift and

moment produced by the trailing-edge flap. This flap was then made to oscillate around its parked position by ± 5 -degrees at various frequencies at a wind speed of 16 m/s; excitation frequency of 2.6 Hz corresponding most closely to flutter conditions. The measured trailing-edge flap's angular position, the lift and moment on the deck are plotted in Figure 22 together with their theoretical counterparts obtained from Theodorsen theory. The loss in the moment coefficient is approximately 50% for both positive (down) and negative (up) flap angles. The loss in lift coefficient is asymmetric. Figure 22 indicates a loss in C_L of $\mathcal{O}(20\%)$ for negative flap angles and a larger loss of $\mathcal{O}(50\%)$ for positive flap angles. This asymmetry is indicative of the effect of the deck's wake on the flap performance, since the flap is more immersed in the thick wake of the deck when deflected downwards. Figure 23 shows a similar behaviour at a number of different frequencies justifying the gain adjustments made to the trailing-edge flap actuator.

VII. CONCLUSIONS

The flexibility and low structural damping of cable-supported bridges make them susceptible to wind-induced motions and dynamic instability. The stabilisation of aeroelastic instabilities, using controllable flaps along the span of the deck has been studied. The effectiveness of various control schemes to suppress/delay flutter was tested for various feedback quantities such as pitch angle, heave displacement and both in combination. A study of a streamlined sectional deck shows that its derivatives are not substantially different from the theoretical derivatives of a thin flat plate. This enabled us to use a theoretical model based on Theodorsen's theory [18] to design controllers that would suppress/delay flutter. By including a wide-ranging experimental programme, this study extends the theoretical results given in [21] and [34]. Starting from a critical flutter velocity of approximately 17.5 m/s, almost all of the controllers tested were able to keep the deck stable up to and well beyond the highest wind velocity tested, which was 20.5 m/s; an increase of over 15%. This was achieved using low-order passive controllers that could, in principle, be replaced by passive mechanical networks that would require little or no servicing. This eliminates the need for a powered computer control systems; a commodity that

is likely to fail during stormy weather conditions when flutter instabilities are most likely to occur. The flutter-suppression performance and robustness of the controllers is confirmed in a turbulent air flow showing that they can also cope with large disturbances.

VIII. ACKNOWLEDGEMENTS

This work was supported by the UK Engineering and Physical Sciences Research Council under grants EP/H029982/1 and EP/H026509/1, and BMT Fluid Mechanics. The support, advice and wind-tunnel time granted by BMT Fluid Mechanics and their staff Stefano Cammelli and Alvin Elliot is gratefully acknowledged. We would also like to thank Professor Tom Wyatt for his many insights and invaluable advice.

REFERENCES

- [1] C. Dyrbye and S. O. Hansen, *Wind Loads on Structures*, 1st ed. Chichester: John Wiley and Sons, 1999.
- [2] M. Schlaich, K. Brownlie, J. Conzett, J. Sobrino, J. Strasky, and K. Takenouchi, "Guidelines for the design of footbridges: Guide to good practice," The International Federation for Structural Concrete, Tech. Rep., 2005.
- [3] K. Y. Billah and R. H. Scanlan, "Resonance, tacoma narrows bridge failure, and undergraduate physics textbooks," *American Journal of Physics*, vol. 59, no. 2, pp. 118–124, 1991.
- [4] A. Larsen, M. Savage, A. Lafreniere, M. C. H. Hui, and S. V. Larsen, "Investigation of vortex response of a twin box bridge section at high and low reynolds numbers," *Journal of Wind Engineering and Industrial Aerodynamics*, vol. 96, pp. 934–944, 2008.
- [5] A. Larsen, S. Esdahl, J. E. Andersen, and T. Vejrum, "Storebølt suspension bridge vortex shedding excitation and mitigation by guide vanes," *Journal of Wind Engineering and Industrial Aerodynamics*, vol. 88, pp. 283–296, 2000.
- [6] M. A. Astiz, "Flutter stability of very long span bridges," *Journal of Bridge Engineering*, vol. 3, no. 3, pp. 132–139, 1998.
- [7] D. Borglund and J. Kuttentkeuler, "Active wing flutter suppression using a trailing edge flap," *Journal of Fluids and Structures*, vol. 16, no. 3, pp. 271–294, 2002.
- [8] E. Burnett, C. Atkinson, B. Sibbitt, B. Holm-Hansen, and L. Nicolai, "NDOF Simulation Model for Flight Control Development with Flight Test Correlation," in *AIAA Modeling and Simulation Technologies Conference*, 2010.
- [9] H. Kobayashi and H. Nagaoka, "Active control of flutter of a suspension bridge," *Journal of Wind Engineering and Industrial Aerodynamics*, vol. 41, pp. 143–151, 1992.
- [10] K. H. Ostenfeld and A. Larsen, "Bridge engineering and aerodynamics: Proceedings of the first international symposium on aerodynamics of large bridges," in *Aerodynamics of Large Bridges*, pp. 3–22, 1992.
- [11] H. I. Hansen and P. Thoft-Christensen, "Active flap control of long suspension bridges," *Journal of Structural Control*, vol. 8, no. 1, pp. 33–82, 2001.
- [12] K. H. Ostenfeld, "A system and a method of counteracting wind induced oscillations in a bridge girder," European Patent EP 0 627 031 B1, 12 June 1996.

- [13] J. M. Corney, "Bridge stabilization," Dec. 4 1997, wO Patent App. PCT/GB1997/001,435. [Online]. Available: <http://www.google.com.ar/patents/WO1997045593A1?cl=en>
- [14] K. Wilde and Y. Fujino, "Aerodynamic control of bridge deck flutter by active surfaces," *Journal of Engineering Mechanics*, vol. 124, no. 7, pp. 718–727, 1998.
- [15] P. Omenzetter, K. Wilde, and Y. Fujino, "Suppression of wind-induced instabilities of a long span bridge by a passive deck-flaps control system part I: Formulation," *Journal of Wind Engineering*, vol. 87, pp. 61–79, 2000.
- [16] —, "Suppression of wind-induced instabilities of a long span bridge by a passive deck-flaps control system part II: Numerical simulations," *Journal of Wind Engineering*, vol. 87, pp. 81–91, 2000.
- [17] H. D. Nissen, P. H. Sorensen, and O. Jannerup, "Active aerodynamic stabilisation of long suspension bridges," *Journal of Wind Engineering*, vol. 92, no. 12, pp. 829–847, 2004.
- [18] T. Theodorsen, "General theory of aerodynamic instability and the mechanisms of flutter," *NACA Report, TR-496*, 1934.
- [19] M. Massaro and J. M. R. Graham, "The effect of three-dimensionality on the aerodynamic admittance of thin sections in free stream turbulence," *Journal of Fluids and Structures*, vol. 57, pp. 81–90, 2015.
- [20] T. Theodorsen and I. E. Garrick, "Nonstationary flow about a wing-aileron-tab combination including aerodynamic balance," *NACA Report, TR-736*, 1942.
- [21] J. Graham, D. Limebeer, and X. Zhao, "Aeroelastic control of long-span suspension bridges," *ASME J. Applied Mechanics*, vol. 78, no. 4, p. pp 041018 (12 pages), 2011.
- [22] K. Wilde, Y. Fujino, and T. Kawakami, "Analytical and experimental study on passive aerodynamic control of flutter of a bridge deck," *Journal of Wind Engineering and Industrial Aerodynamics*, vol. 80, no. 1??2, pp. 105 – 119, 1999.
- [23] N.M.I, "The aerodynamic stability of the Humber suspension bridge platform at various erection stages," National Maritime Institute, NMI, Tech. Rep., 1977.
- [24] J. M. R. Graham, D. J. N. Limebeer, and X. Zhao, "Aeroelastic modelling of long-span suspension bridges," in *Proc. of the 18th IFAC World Congress*, Milan, Italy, pp. 9212 – 9217, 2011.
- [25] R. L. Bisplinghoff, H. Ashley, and R. L. Halfman, *Aeroelasticity*. Addison-Wesley, 1955.
- [26] S. Evangelou, D. J. N. Limebeer, R. S. Sharp, and M. C. Smith, "Steering compensators for high-performance motorcycles," *ASME J. Applied Mechanics*, vol. 74, no. 5, pp. 332–346, 2007.
- [27] M. Green and D. J. N. Limebeer, *Linear Robust Control*. Englewood Cliffs, New Jersey: Prentice Hall, 1995.
- [28] The Mathworks Inc., *MATLAB 6 Reference Manual*, 2000. [Online]. Available: <http://www.mathworks.com>
- [29] J. D. Holmes, *Wind Loading of Wind Structures*. CRC Press, 2015.
- [30] A. Selberg, "Oscillation and aerodynamic stability of suspension bridges," *Civil Engineering and Construction Series*, vol. 13, 1961.
- [31] X. Zhao, K. Gouder, J. Graham, and D. Limebeer, "Buffet loading, dynamic response and aerodynamic control of a suspension bridge in a turbulent wind," 2015, submitted for publication.
- [32] R. H. Scanlan and J. J. Tomko, "Airfoil and bridge deck flutter derivatives," *Journal of Engineering Mechanics*, vol. 97, no. 6, pp. 1717–1737, 1971.
- [33] M. Matsumoto, "Aerodynamic damping of prisms," *Journal of Wind Engineering and Industrial Aerodynamics*, vol. 59, pp. 159–175, 1996.
- [34] D. J. N. Limebeer, J. M. R. Graham, and X. Zhao, "Buffet suppression in long-span suspension bridges," *Annual Reviews in Control*, vol. 35, pp. 235–246, 2011.



research interests include flow control for drag reduction and fluid-structure interactions.



University of Oxford for three years before joining Warwick. His research interests include the control of fluid-structure interactions, coupled infinite-dimensional systems and wind energy.



include the theory and application of robust control, the dynamics and control of road vehicles and the control of aeroelastic phenomena.



methods including application to the dynamics of floating bodies and of flexible structures in the natural wind.

Kevin Gouder graduated from the University of Malta with a B.Eng. (Hons.) in Mechanical Engineering in 2002, after which he spent two years in industry. He graduated from Imperial College London with an MSc in Computational Fluid Dynamics in 2005 and a PhD in Experimental Fluid Dynamics in 2010. He is currently a teaching fellow in the Department of Aeronautics at Imperial College. His current

Xiaowei Zhao is a Global Research Fellow/Senior Research Fellow at the University of Warwick. He obtained a BEng degree in Automatic Process Control from Beijing University of Chemical Technology in 2003. He then obtained MSc and PhD degrees in Control Systems and Control Theory in 2004 and 2009; both from Imperial College London. After that he worked as a postdoctoral researcher at the

David J. N. Limebeer has been the professor of Control Engineering at the University of Oxford since 2009. He was Head of the Control and Power group and the Department of Electrical and Electronic Engineering at Imperial College between 1996 and 1999, and between 1999 and 2009, respectively. He is a Fellow of the IEEE and the Royal Academy of Engineering. His current research interests

J Michael R Graham is professor of aerodynamics in the Aeronautics Department at Imperial College; he was Head of Department from 1999 to 2003. He has a Mathematics degree from Cambridge University followed by a PhD in Aeronautical Engineering from the University of London (Imperial College). His main areas of research have been in low speed, unsteady flows and associated vortex